Alternative Bridge Spoke Permanent Magnet Synchronous Generator Design for Wind Power Generation Systems

DONG-HO KIM[1], **(Student Member, IEEE), KWANG SOO KIM**[2], **(Member, IEEE),**
IN-JUN YANG[1], **(Student Member, IEEE), JU LEE**[1], **(Senior Member, IEEE),**
AND WON-HO KIM[3], **(Member, IEEE)**
[1]Department of Electrical Engineering, Hanyang University, Seoul 04763, South Korea
[2]Department of Smart Mobility Engineering, Halla University, Wonju 26404, South Korea
[3]Department of Electrical Engineering, Gachon University, Seongnam 13120, South Korea

Corresponding author: Won-Ho Kim (wh15@gachon.ac.kr)

ABSTRACT Generators are a key technological element of wind power generation systems. The use of synchronous generators that employ heavy rare-earth permanent magnets is increasing owing to the demand for higher efficiencies. However, these magnets are expensive and undergo an unbalanced supply and demand. Therefore, spoke-type structures have been developed and used in various fields to compensate for the deficient performance when using a ferrite magnet, which is inexpensive and provides a stable supply and demand. However, permanent magnet synchronous generators (PMSGs) with adopted spoke-type structures and an output power of 1 kW or higher have not been studied and practically applied sufficiently. Additionally, new designs must consider differences between the target specifications of a generator and wind turbine. In this study, we designed and analyzed the characteristics of an alternative bridge spoke-type PMSG modeling a generator for a 3-kW class wind turbine. We analyzed the performance of the existing spoke-type generator and proposed an alternative bridge spoke shape with an improved performance by removing the leakage flux of the bridge. The performance of the existing spoke model was compared using the finite element method (FEM), and the performance of the proposed model was verified more accurately by performing a three-dimensional (3D) analysis considering the 3D effect. Additionally, we analyzed the voltage fluctuation rate according to the number of stator slots and overhang structure and designed a final model. Considering the characteristics of the ferrite magnet used in the spoke-type design, the irreversible demagnetization characteristics of the conventional and final models were compared using simulations, followed by a comparison between the stiffness characteristics of the two models. Finally, a prototype was manufactured, and the feasibility of the final design was verified using the performance tests.

INDEX TERMS Permanent magnet synchronous generator (PMSG), spoke-type ferrite magnet synchronous generator (SPMSG), rotor overhang, wind turbine.

I. INTRODUCTION

Recently, interest in and studies on renewable energy, particularly on ecofriendly and economic wind power systems, have been continually growing [1]–[6]. Generators are a key technological element of a wind power generation system because their performance can directly reduce the weight and

The associate editor coordinating the review of this manuscript and approving it for publication was Guido Lombardi.

increase the efficiency of the corresponding wind power generation system. Many generators, such as switched reluctance and induction generators, have been used; however, the use of permanent magnet synchronous generators (PMSGs) is increasing owing to their high output density per unit volume and the possibility to be miniaturized [7]–[10]. The permanent magnet types employed in PMSGs are ferrite and heavy rare-earth magnets. Heavy rare-earth magnets with a high energy density are preferred because of their high efficiency;

TABLE 1. Comparison of characteristics with PMSG.

Parameter	IPMSM	SPMSM	Conventional Spoke	Alternative bridge Spoke
Shape				
THD	High	Low	High	low
Cogging Torque	High	middle	High	low
Torque	High	Low	Middle	middle

however, their supply and demand are unstable and expensive [11], [12]. The supply and demand of ferrite magnets are stable in addition to their lower cost compared with that of rare-earth magnets. However, ferrite magnets have a low magnetic flux density, which is approximately one-third that of rare-earth magnets, making it difficult for them to achieve the same performance as rare-earth magnets. Therefore, a spoke-type structure was developed to overcome the problem of low magnetic flux density. Therefore, spoke-type structures have been widely studied and commercialized in permanent magnet synchronous motors (PMSMs) [13]–[17]. In particular, many studies are being actively conducted on the spoke-type PMSMs for different applications, such as shape studies to improve demagnetization or magnetization performance, and performance maximization using an asymmetric structure and barrier design in the rotor core, use of magnetic materials applied with new materials [18]–[25]. However, the research and development and application cases of the spoke-type structure are still insufficient for 1-kW or highergenerators [26]–[30]. Although structures of the spoke-type PMSMs and a PMSGs are similar, the required specifications are distinct. In particular, the cogging torque, voltage fluctuation rate during load operation, and efficiency for wind turbines are extremely important design specifications. In addition, the cogging torque is directly associated with the starting performance. Therefore, the voltage fluctuation rate and cogging torque must be reduced for a spoke-type PMSG with a large leakage magnetic flux in the axial direction. In this study, we investigated the design and characteristics of an alternative bridge spoke-type PMSG for use in wind turbines. The alternative bridge spoke-type PMSG is designed using a 3-kW-class PMSG as a model. Subsequently, the performance of an existing spoke-type and that of the proposed alternative bridge PMSG were compared using the finite element analysis (FEA) method. Additionally, an accurate 3D analysis was conducted considering three-dimensional (3D) effects, such as the spoke-type axial leakage magnetic flux, and the performance changes were examined. The proposed model was designed by analyzing the stiffness according to the number of stator slots and overhangs for the voltage drop characteristics. Table 1 demonstrates that the characteristics of the proposed alternative bridge spoke-type PMSG are

superior to those of the existing permanent magnet rotor shapes.

Considering the no-load and load characteristics of the proposed model and those of the permanent magnet material (ferrite), the irreversible demagnetization and stiffness characteristics of the existing and proposed models were compared using simulation. Finally, prototypes were manufactured, and performance tests were performed to verify the validity of the proposed design and characterization.

II. ALTERNATIVE BRIDGE SPOKE-TYPE PMSG
A. PMSG PRINCIPLE AND EQUIVALENT CIRCUIT
The PMSG has the same structure as the PMSM; however, a difference exists in whether the input is mechanical or electrical energy. As the input mechanical energy rotates the generator shaft, the magnetic flux generated by the permanent magnet in the rotor generates an induced electromotive force in the armature coil. In addition, when stator is connected to a load, current flows. In PMSGs, the no-load electromotive force E_0 arising from the magnetic flux generated by the permanent magnet and the armature reaction electromotive force e_a generated by the armature reaction magnetic flux are induced. Furthermore, e_a can be obtained as follows [31]–[33]:

$$e_a = -\frac{d\lambda_a}{dt} = -N\frac{d\phi_a}{dt} = -L_a\frac{di_a}{dt} \quad (1)$$

where λ_a is the armature reaction flux linkage, ϕ_a is the armature reaction flux, and N is the number of turns. Equation 1 can be expressed as the armature reaction electromotive force phasor E_a in the frequency domain as follows:

$$E_a = jX_aI_a \quad (2)$$

where X_a is the armature reaction reactance. If leakage flux exists in a PMSG, the induced electromotive force E_l is expressed as follows: where

$$E_l = jX_lI_a \quad (3)$$
$$X_s = X_a + X_l$$
$$Z_s = jX_s + R_a \quad (4)$$

where X_l is the leakage reactance. In Equation 4, the sum of X_a and X_l is called the synchronous reactance X_s, and the sum of X_s and Ra is called the synchronous impedance Z_s.

The voltage V on the terminal side of the generator is obtained by subtracting the voltage drop owing to the synchronous reactance X_s and the voltage drop owing to the winding resistance R_a from the no-load induced electromotive force E_0, which is the same as that expressed in Equation 5. Fig. 1 presents the equivalent circuit for one phase of a PMSG.

$$V = E_0 - jX_sI_a - R_aI_a \quad (5)$$

In the rotor that generates the no-load counter electromotive force E_0 of the equivalent circuit, the magnetic arrangement torque acts in the opposite direction to the rotational
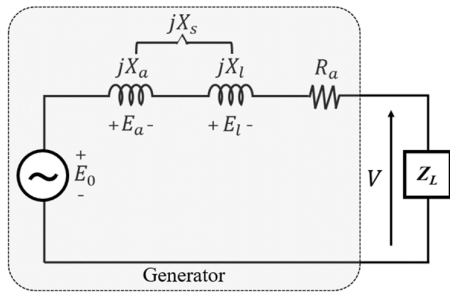
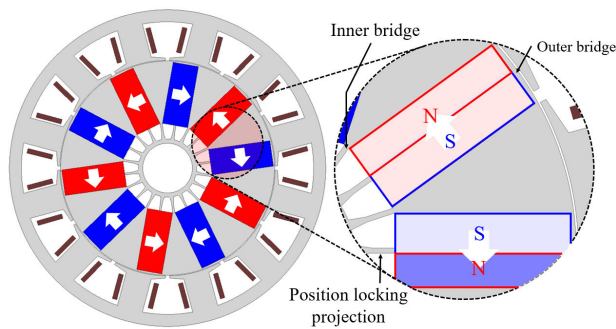**FIGURE 1.** Schematic equivalent circuit of synchronous generator.

FIGURE 2. Cross-section of conventional spoke-type PMSG.

TABLE 2. Specifications of a 3-kW spoke-type PMSG.

Parameter	Value	Unit
Power	3	kW
Speed	300	rpm
Voltage	210 ↑	V$_{rms}$
Voltage fluctuation rate	10 ↓	%
Current	9 ↓	A$_{rms}$
Efficiency	92	%
Cogging Torque	5	Nm

direction of the field. Therefore, a power is needed to overcome the self-arranged torque generated in the direction opposite to the rotational direction and return it to a constant speed. Equation 6 expresses the power per phase considering the electrical and mechanical losses.

$$P_e = T_G \omega_s - P_{loss} = V I_a \cos\theta \qquad (6)$$

Moreover, P_{loss} is the sum of the electrical and mechanical losses, and the torque applied to the rotor is expressed as

$$T_G = \frac{V I_a \cos\theta + P_{loss}}{\omega_s} \qquad (7)$$

B. CONVENTIONAL SPOKE-TYPE PMSG

Table 2 lists the target specifications of a PMSG for a 3-kW-class wind turbine. Fig. 2 shows a 10-pole 12-slot PMSG using a conventional spoke-type rotor designed using the voltage and output power equations.
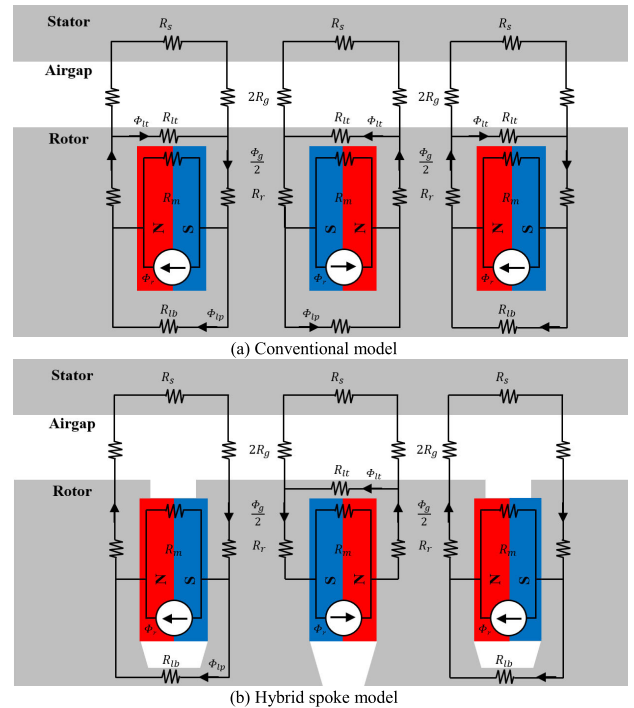

FIGURE 3. Magnetic equivalent circuits (a) conventional and (b) alternative bridge spoke models.

The conventional spoke-type rotor consists of a permanent magnet and a pole piece, an inner bridge to connect it to the shaft, a position-locking projection to fix the position of the magnet, and an outer bridge to prevent the magnet from scattering. Fig. 3(a) shows a conventional spoke-type magnetic circuit, where Φ_g is the airgap magnetic flux, Φ_m is the magnetic flux, and Φ_s and Φ_r are the magnetic fluxes of the stator and rotor, respectively. R_m is the magnetic resistance of the magnet, R_s and R_r are the magnetic resistances of the stator and rotor, respectively, and R_g is the magnetic resistance of the air gap. Φ_{lo}, Φ_{li}, and Φ_{lp} are the leakage fluxes flowing through the outer, inner, and position locking projections, respectively. In addition, R_{lo}, R_{li}, and R_{lp} are the corresponding magnetic resistances. Each bridge is structurally necessary because it fixes the pole piece and the magnet, and prevents scattering; however, it reduces the electromagnetic performance because of the generation of a leakage magnetic flux, as shown in Fig. 3(a). In addition, the magnetization performance of a spoke-type rotor is important, and the position locking projection interferes with the magnetization of the lower part of the magnet. In general, the inner and outer bridges are designed to be as narrow as possible to induce magnetic saturation, which helps reduce the leakage magnetic flux. Concurrently, as the thickness of a bridge decreases, the rigidity becomes disadvantageous during operation; thus, the bridge thickness reduction is limited.

R_m is the magnetic resistance of the magnet, R_s and R_r are the magnetic resistances of the stator and rotor, respectively, and R_g is the magnetic resistance of the air gap. Φ_{lo}, Φ_{li}, and
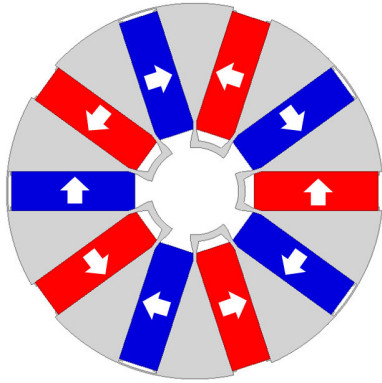
FIGURE 4. Cross-section of Alternative bridge spoke-type rotor.

FIGURE 5. Comparison of no-load line voltages of the conventional and alternative bridge spoke-type models.

Φ_{lp} are the leakage fluxes flowing through the outer, inner, and position locking projections, respectively. In addition, R_{lo}, R_{li}, and R_{lp} are the corresponding magnetic resistances. Each bridge is structurally necessary because it fixes the pole piece and the magnet, and prevents scattering; however, it reduces the electromagnetic performance because of the generation of a leakage magnetic flux, as shown in Fig. 3(a). In addition, the magnetization performance of a spoke-type rotor is important, and the position locking projection interferes with the magnetization of the lower part of the magnet. In general, the inner and outer bridges are designed to be as narrow as possible to induce magnetic saturation, which helps reduce the leakage magnetic flux. Concurrently, as the thickness of a bridge decreases, the rigidity becomes disadvantageous during operation; thus, the bridge thickness reduction is limited.

FIGURE 6. Comparison of cogging torques of conventional and Alternative bridge spoke-type models.

C. ALTERNATIVE BRIDGE SPOKE-TYPE DESIGN

Unlike the conventional spoke-type structure, in the alternative bridge spoke-type structure, only half of the inner and outer bridges are used, and the scattering of the pole pieces or the permanent magnet is prevented in the intersection of the inner and outer bridges. In addition, by making an angular inside for the rotor and developing an optimal design, the magnet was fixed without a position-locking projection. The corresponding alternative bridge spoke-type magnetic circuit is shown in Fig. 3(b), where R_{go} and R_{gi} are the magnetic resistances of the outer and inner airgaps, respectively, and Φ_{go} and Φ_{gi} are the corresponding leakage fluxes.

The two-dimensional (2D) FEA was conducted to validate the performance of the proposed alternative bridge spoke model, and its performance was compared with that of the conventional spoke-type model. To this end, the outer and inner diameters, and air gap of the stators and rotors, and the number of magnets used in both models were identical. Fig. 5 shows the line voltage of each model under no-load conditions. Fig. 6 displays the cogging-torque waveforms of each model.

The alternative bridge spoke model significantly reduced the leakage magnetic flux owing to the conversion of half of
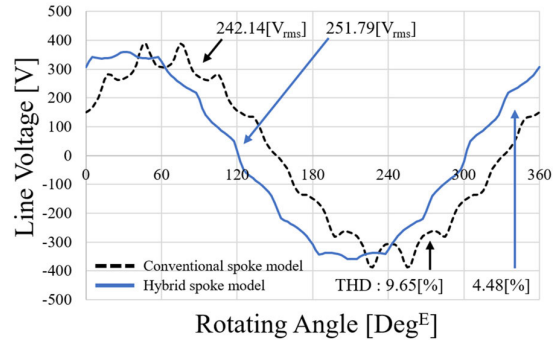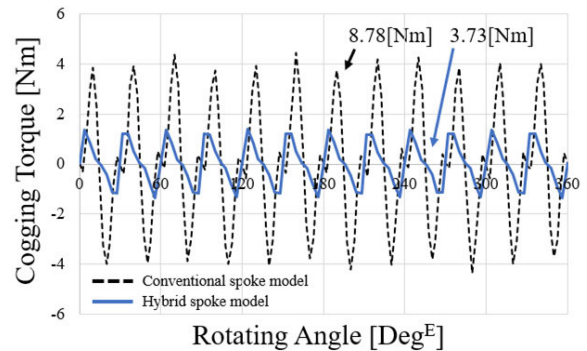
the outer bridges into voids, as shown in Fig. 3(b). Similarly, half the number of inner bridges exist, as shown in Fig. 3(b). Moreover, fixing the magnet without a supporting structure blocked the leakage magnetic flux generated in the position-locking projection. A decrease in the leakage magnetic flux increased the back electromotive force between the no-load lines of the alternative bridge model by approximately 4.0% compared to that in the existing spoke-type model. Furthermore, total harmonic distortion (THD) of the line back EMF improved from 9.6 to 4.48%. Because the number of outer bridges was reduced by half and the thickness was minimized in the alternative bridge model, changes in the reluctance were also minimized, reducing the cogging torque by approximately 47.1% compared to that of the existing spoke-type model. Table 3 presents a performance comparison of the two models for power generation.

The alternative bridge spoke model increased the power generation voltage by approximately 5.3% when the output is 3 kW, which could be attributed to the reduction in both the leakage flux and current owing to the removal of the bridges. In addition, because current reduction reduces copper loss, the alternative bridge spoke-type model exhibited an increase of 0.2% efficiency compared to the conventional model. Moreover, the voltage fluctuation rate of the

TABLE 3. Performance under load conditions.

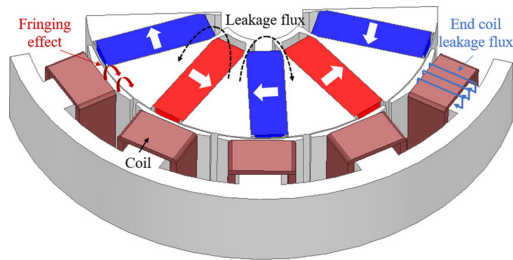| Parameter	Conventional spoke model	Alternative bridge spoke model	Unit
Voltage	127.69	134.52	V_{rms}
Line Voltage	219.4	231.1	V_{rms}
Current	7.92	7.62	A_{rms}
Torque	116.94	100.24	Nm
Voltage fluctuation rate	9.4	8.24	%
Output Power	3032.43	3076.02	W
Efficiency	95.49	95.69	%

FIGURE 7. 3D modeling of Alternative bridge spoke-type PMSG.

TABLE 4. 2D and 3D FEA analysis results.

	Parameter	2D model	3D model	Unit
No-Load	Line Voltage	251.79	247.55	V_{rms}
	Cogging Torque	3.73	2.1	Nm
Load	Line Voltage	231.1	206.87	V_{rms}
	Current	7.62	8.24	A_{rms}
	Torque	100.24	97.6	Nm
	Voltage fluctuation rate	8.98	16.43	%
	Output Power	3076.02	2991.56	W
	Efficiency	95.69	95.18	%

alternative bridge mode, which is an significant specification, was also improved over the existing model.

III. DESIGN CONSIDERING 3D EFFECT
A. THREE-DIMENSIONAL MODELING AND PERFORMANCE ANALYSIS
An accurate 3D performance analysis was conducted considering 3D effects, such as the rotor axial and end coil leakage fluxes generated in a spoke structure, and the fringing effect in the airgap. Fig. 7 illustrates a schematic of the 3D shape of the alternative bridge spoke-type model.

The results of the 3D and 2D FEA of the alternative bridge spoke model are summarized in Table 4. The 2D and 3D analysis results were similar under the no-load condition. However, the 2D and 3D analysis results differed during the power generation operation because the 3D effects were not reflected in the 2D analysis. Moreover, a large voltage drop occurs during power generation owing to the 3D effects, and the voltage and voltage fluctuation rates are not satisfied, as defined in the target specifications.

TABLE 5. Phase resistance and number of turns for each slot model.

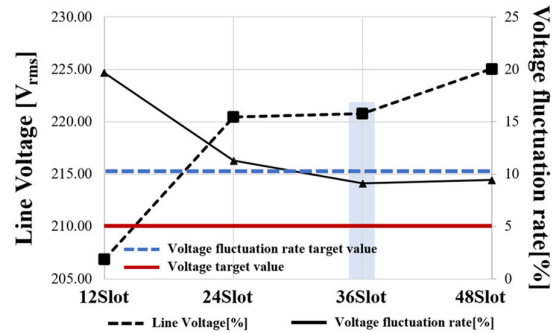| Parameter	12 Slot	24 Slot	36 Slot	48 Slot
Number of Turns	91	43	31	23
Phase Resistance [Ω]	0.57	0.53	0.58	0.67

FIGURE 8. Line voltage and voltage fluctuation rate.

In PMSGs, electric current flows in the stator coil during power generation, and the resulting magnetic flux of the armature reaction flows through the stator core, airgap, and rotor core. The magnetic path between the stator and rotor has a magnetic flux component in the radial direction and an axial magnetic flux component generated by the fringing effect. The axial magnetic flux component, which cannot be considered in the 2D analysis, is reflected in the 3D analysis, resulting in a reduction in the total magnetoresistance of the armature reaction. Therefore, during load operation, the magnitude of the armature reaction in the 3D analysis (and not in the 2D analysis) increases. Therefore, the voltage generated during the load operation decreases in the 3D analysis compared to that of the 2D analysis because of an increase in the magnitude of the armature reaction. The armature reaction is an inductance component in a self-equivalent circuit, and the inductance is proportional to the square of the number of turns. Therefore, an additional design to reduce the number of turns is required to improve the voltage drop owing to the armature reaction.

B. REDUCING VOLTAGE DROP
We developed a design to reduce the number of turns required to meet the target specifications by reducing the voltage drop. First, we increased the number of stator slots, changed the winding method and the number of turns, and examined the trend. We examined 12, 24, 36, and 48 stator slots, for each of which the phase resistances and number of turns are listed in Table 5.

Fig. 8 demonstrates the line voltage and voltage fluctuation rate based on a 3-kW output and considering changes in the stator phase resistance with changes in the number of slots.

Fig. 9 shows the copper losses and efficiencies. The number of turns decreases as the stator slots increase for an output of 3 kW. The magnitude of the armature reaction decreases as
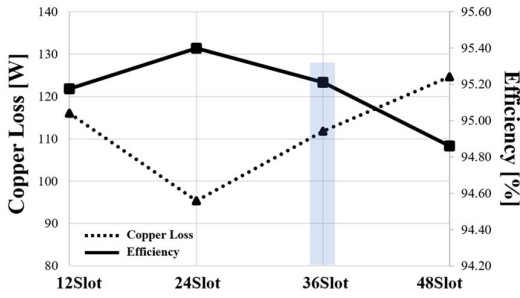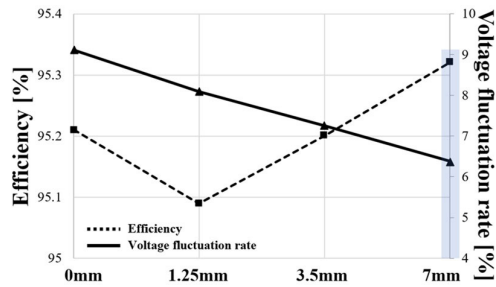
FIGURE 9. Copper loss and efficiency.

FIGURE 10. Efficiency and voltage fluctuation rate variation with overhang length.

TABLE 6. Model specifications.

	Parameter	Value	Unit
Stator	Number of Slots	36	-
	Outer Diameter	420	mm
	Inner Diameter	286	mm
	Stack Length	73	mm
Winding	Coil Diameter	1.0	mm
	Turns	26	-
Rotor	Number of Poles	10	-
	Outer Diameter	284	mm
	Inner Diameter	66	mm
	Stack Length	84	mm
	Airgap	1	mm

(a) Alternative bridge spoke generator with overhang 1/2 model

(b) Alternative bridge spoke type generator core flux density plot
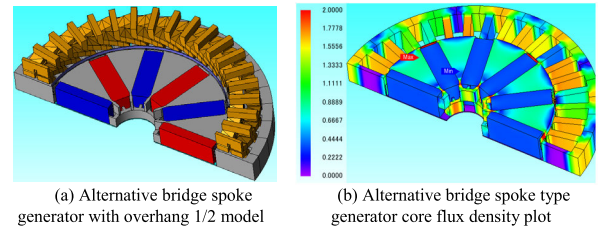
FIGURE 11. Final model shape and magnetic flux density plot.

(a) Comparison of B-H curves among different PM materials

(b) B-H curve according to the temperature of ferrite magnet
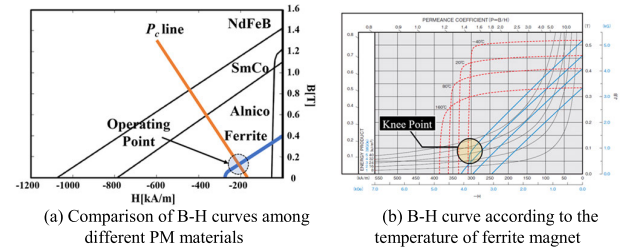
FIGURE 12. B-H curve characteristics of ferrite magnets.

the number of turns decreases. As the number of stator slots increases, the voltage fluctuation rate decreases. Conversely, the magnitude of the voltage increases during load operation. When the number of slots increases, the size of the phase resistance increases owing to an increase in the number of end turns, and the current decreases, thereby increasing the efficiency. Therefore, 36 and 48 slots satisfy the voltage fluctuation rate, as specified in the target specifications. Thus, the 36-slot model with an excellent efficiency and manufacturability was selected. Rotor overhangs of 1.25, 3.5, and 7 mm were applied as one-sided standards, and the trend was determined by conducting 3D FEA. Fig. 10 shows the voltage fluctuation rate and efficiency variation with the overhang length.

As the length of the overhang increases, the number of turns is reduced because both the number of magnets used and the flux linkage increase. The voltage fluctuation rate decreases owing to a decrease in the number of turns as the overhang length increases, and the efficiency increases because of the copper loss owing to a decrease in the number of turns. A 36-slot model with an overhang of 7 mm was selected as the final model.

IV. COMPARISON OF DEMAGNETIZATION AND MECHANICAL RIGIDITY USING SIMULATION

A. COMPARISON OF THE DEMAGNETIZATION CHARACTERISTICS

The current generated by the wind creates an armature reaction flux and flows toward the load. A current larger than the rated current may flow owing to the size of the load

resistance or failure. Thus, the magnitude of the armature reaction force and magnetic flux increases in proportion to the current, which affects the irreversible demagnetization of the magnet. Fig. 12 shows that the operating point of the permanent magnet device is determined at the point where the B-H curve of the permanent magnet and the P_C line intersect.

The P_C line is determined by the shape of the permanent magnet machine as follows:

$$P_c = \frac{-B_m}{\mu_0 H_m} = \frac{l_m}{g} \frac{1}{C_\phi} \tag{8}$$

$$C_\phi = \frac{A_m}{A_g} \tag{9}$$

where $B_m = \phi/A_m$, $H_m = F_m/l_m$, l_m is the magnet length, A_m is the magnet area, A_g is the airgap area, and g is the airgap length. In addition,

$$F_m = \frac{-\phi_r}{P_m + P_g} \tag{10}$$

$$P_g = \mu_0 A_g/g, \quad P_m = \mu_0 A_m/l_m \tag{11}$$

where F_m is the magnetomotive force. As the current increases, the component of the armature reaction increases,
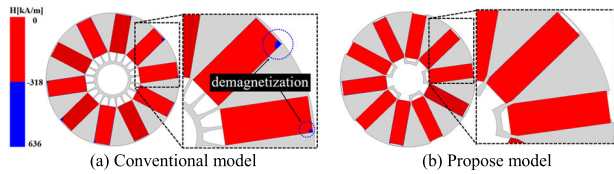
FIGURE 13. Comparison of results of irreversible demagnetization of the conventional model and the proposed model.

and the *Pc* line moves to the left. Irreversible demagnetization occurs when the operating point is formed below the knee point. In particular, ferrite magnets have a low coercive force compared to rare-earth permanent magnets (NdfeB, SmCo); thus, they are vulnerable to demagnetization by a reverse magnetic field, where demagnetization occurs at low temperatures [34]–[37]. The current density of the proposed model is approximately 2 A/mm^2 and the operating temperature is in the range of 20–50 °C; thus, permanent magnet irreversible demagnetization by temperature does not occur. Subsequently, the demagnetization characteristics of the existing model and the proposed model owing to the armature reaction were compared using simulation. The demagnetization current owing to a fault is twice that of the existing rated current. Fig. 13 illustrates the irreversible demagnetization area according to the shape of the rotor.

The amount of permanent magnet used in both models is approximately the same; however, it can be confirmed that irreversible demagnetization of the conventional spoke model occurred in some areas of the permanent magnet. Unlike the conventional spoke model, an irreversible demagnetization area did not occur in the proposed alternative bridge spoke-type model by removing the external bridge or applying a barrier. This is because the removal of outer bridge and the application of an air gap barrier makes the magnetic resistance on the outer diameter side of the rotor be higher than that of the conventional spoke model, which leads to be more robust to reverse magnetic fields.

B. COMPARISON OF THE MECHANICAL RIGIDITY

The mechanical stiffness characteristics during road load operation are compared because the shapes of the existing and proposed models are different. The mechanical stiffness characteristics are compared with the maximum value of the equivalent stress that can occur in the model and the safety factor. The maximum value of the equivalent stress indicates the maximum stress that can occur in the model. The safety factor is an index that guarantees structural stability against uncertainties caused by various factors. Although the safety factor standard varies depending on the design, it usually has a value of 2 or more, as expressed in Equation (12).

$$\alpha_{sf} = \frac{Tensile\ yield\ strength}{Peak\ Stress} \qquad (12)$$

Fig. 14 presents a comparison between the rigidity of the conventional and final models. The equivalent stresses of the conventional and proposed models are 249.43 and
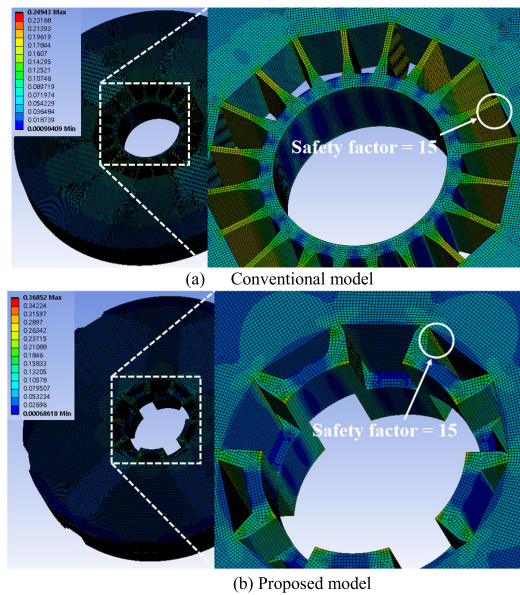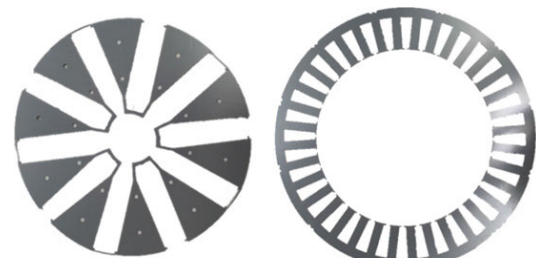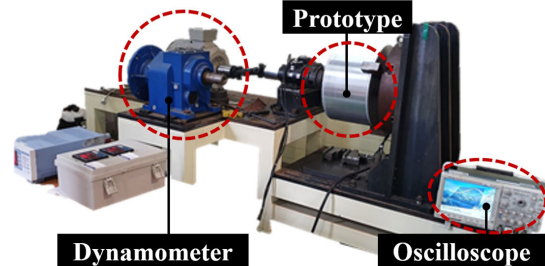

FIGURE 14. A comparison between the rigidity of the conventional and proposed models.

FIGURE 15. Photographs of Generator prototype core and test system.

368.52 kPa, respectively. Therefore, the final model is disadvantageous in terms of the mechanical rigidity. However, the safety factor is 15 for both models. As the safety factor of the final model is similar to that of the existing mass-produced model, the rigidity of the final model has no problem, and thus no abnormality exists in the production result.

V. EXPERIMENTAL WORK AND RESULTS

A prototype generator was manufactured to verify the design and performance of the designed generator, and its performance was examined. Fig. 15(a) shows the manufactured
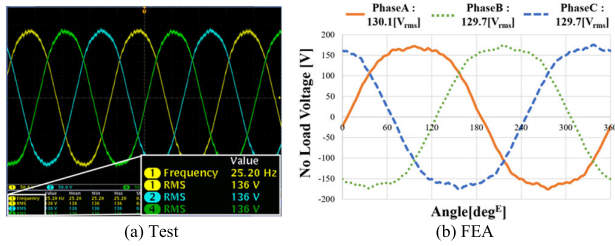
FIGURE 16. No-load phase back EMF @ 300rpm (a) Test (b) FEA.

TABLE 7. Comparison of experimental and simulation results.

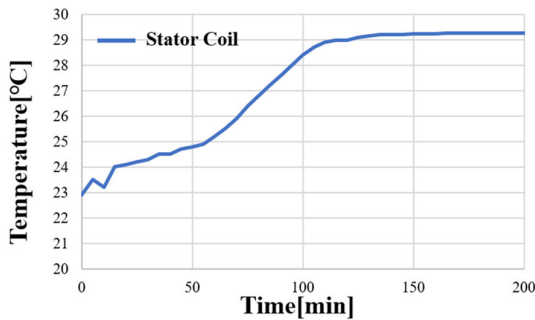|	Parameter	Proposed Model FEA	Test	Unit
No-Load	Line Voltage	232.10	230.99	V_{rms}
	THD	1.64	0.55	%
	Cogging Torque	2.7	2.5	Nm
Load	Line Voltage	218.17	212.79	V_{rms}
	Current	7.92	8.66	A_{rms}
	Torque	103.64	107.31	Nm
	Voltage Fluctuation Rate	6.38	8.43	%
	Output Power	2998.42	3160	W
	Efficiency	95.3	93.7	%

FIGURE 17. Temperature test graph during load operation.

stator and rotor, and Fig. 15(b) presents the test configuration of the generator prototype and dynamometer.

In the tests, the no-load back electromagnetic force, cogging torque, voltage, current, and torque at a rated operating speed of 300 rpm were measured. Fig. 16 presents the measured waveform using an oscilloscope and the no-load back EMF waveform analyzed using FEA. According to the comparison results, the error in the size of the effective value was approximately 5%, indicating a high accuracy.

Table 7 presents a comparison between the experimental and simulation results for the prototype.

The test was performed at an environmental temperature of 20°C, and the Fig.17 is a graph measuring the temperature rise during load operation. The temperature sensor is attached to the stator winding side, and due to the low current density, it can be seen that the temperature saturation appears at about 30°. The load resistance was 14.3 Ω, and the resulting measured output power was 3.16 kW. Table 7 confirms that most of the performance results during the no-load and load operations are comparable with the FEA results. How-

ever, the current was slightly higher than that of the FEM analysis, which slightly increased the output based on the load resistance setting during the test. Therefore, current and torque were slightly increased. In addition, the efficiency decreased owing to an increase in the iron loss, which is attributed to the harmonic iron loss and analysis error.

Except for the above cases, the simulation and experimental results were comparable, validating the design and performance of the proposed alternative bridge spoke model.

VI. CONCLUSION

This study performed a design and characteristic analysis of an alternative bridge spoke-type PMSG. In contrast to the conventional spoke type, a crossroad bridge was applied, and the support structure was eliminated to minimize the leakage magnetic flux. Therefore, a higher line voltage and lower cogging torque than those of the existing spoke-type model were achieved. In addition, 3D FEA analysis confirmed that the voltage fluctuation rate was higher than that of the 2D analysis owing to the 3D effect, and the final model, to which an overhang was applied, was selected by analyzing the performance trend based on the number of stator slots and overhang. This is to reduce the voltage drop owing to the armature reaction because the armature reaction component is proportional to the square of the number of turns. The final model was selected by changing the number of turns according to the number of slots and reducing the number of turns using overhangs to improve the voltage drop and examine other performance parameters, such as current and efficiency. The final model improved the voltage fluctuation rate by more than 8% compared to the existing model and satisfied all target specifications. In addition, considering the characteristics of permanent magnets, irreversible demagnetization was compared using simulation. It was confirmed that the proposed model is stronger in irreversible demagnetization than the existing model. Considering the changes in the rotor shape, the mechanical stiffness was also compared with that of the existing model. Although the maximum stress was slightly increased, the stiffness characteristics were comparable to those of the existing model, and the safety factor was checked to confirm that there was no problem in mechanical stiffness even during load operation. Finally, a prototype was manufactured, and a performance test was conducted to verify the validity of the design and analysis results. The results obtained in this study will be helpful for accurate characterization and design of low- and medium-capacity generators. In addition, the proposed model is expected to contribute toward applied research in various fields.

REFERENCES

[1] K.-J. Ko, S.-M. Jang, J.-H. Park, H.-W. Cho, and D.-J. You, "Electromagnetic performance analysis of wind power generator with outer permanent magnet rotor based on turbine characteristics variation over nominal wind speed," *IEEE Trans. Magn.*, vol. 47, no. 10, pp. 3292–3295, Oct. 2011.

[2] Y. Gu, Y. Huang, Q. Wu, C. Li, H. Zhao, and Y. Zhan, "Isolation and protection of the motor-generator pair system for fault ride-through of renewable energy generation systems," *IEEE Access*, vol. 8, pp. 13251–13258, 2020.

[3] Y. Fang, K. Jia, Z. Yang, Y. Li, and T. Bi, "Impact of inverter-interfaced renewable energy generators on distance protection and an improved scheme," *IEEE Trans. Ind. Electron.*, vol. 66, no. 9, pp. 7078–7088, Sep. 2019.

[4] M. H. Zamani, G. H. Riahy, and M. Abedi, "Rotor-speed stability improvement of dual stator-winding induction generator-based wind farms by control-windings voltage oriented control," *IEEE Trans. Power Electron.*, vol. 31, no. 8, pp. 5538–5546, Aug. 2016.

[5] X. Yang, D. Patterson, and J. Hudgins, "Permanent magnet generator design and control for large wind turbines," in *Proc. IEEE Power Electron. Mach. Wind Appl.*, Jul. 2012, pp. 1–5.

[6] J. Lee, G. Seo, J. Mun, M. Park, and S. Kim, "Thermal and mechanical design for refrigeration system of 10 MW class HTS wind power generator," *IEEE Trans. Appl. Supercond.*, vol. 30, no. 4, pp. 1–5, Jun. 2020.

[7] Y. Chen, P. Pillay, and A. Khan, "PM wind generator comparison of different topologies," in *Proc. Conf. Rec. IEEE Ind. Appl. Conf., 39th IAS Annu. Meeting.*, vol. 3, Oct. 2004, pp. 1405–1412.

[8] M. A. Khan, P. Pillay, and M. Malengret, "Impact of direct-drive WEC systems on the design of a small PM wind generator," in *Proc. IEEE Bologna Power Tech. Conf.*, vol. 2, Jun. 2003, p. 7.

[9] Wang, H. Qingming, B. Jianlong, and P. Jian, "Study on control system of low speed PM generator direct driven by wind turbine," in *Proc. Int. Conf. Electr. Mach. Syst.*, vol. 2, 2005, pp. 1009–1012.

[10] Z. Wu, X. Dou, J. Chu, and M. Hu, "Operation and control of a direct-driven PMSG-based wind turbine system with an auxiliary parallel grid-side converter," *Energies*, vol. 6, no. 7, pp. 3405–3421, Jul. 2013.

[11] H. Tahanian, M. Aliahmadi, and J. Faiz, "Ferrite permanent magnets in electrical machines: Opportunities and challenges of a non-rare-earth alternative," *IEEE Trans. Magn.*, vol. 56, no. 3, pp. 1–20, Mar. 2020.

[12] X. Zhu, L. Wang, Y. Chen, L. Chen, and L. Quan, "A non-rare-earth doubly salient flux controllable motor capable of fault-tolerant control," *IEEE Trans. Magn.*, vol. 51, no. 11, pp. 1–4, Nov. 2015.

[13] M. Barcaro and N. Bianchi, "Interior PM machines using ferrite to replace rare-earth surface PM machines," *IEEE Trans. Ind. Appl.*, vol. 50, no. 2, pp. 979–985, Mar. 2014.

[14] A. Fasolo, L. Alberti, and N. Bianchi, "Performance comparison between switching-flux and IPM machines with rare-earth and ferrite PMs," *IEEE Trans. Ind. Appl.*, vol. 50, no. 6, pp. 3708–3716, Nov./Dec. 2014.

[15] S. G. Lee, J. Bae, and W.-H. Kim, "A study on the maximum flux linkage and the goodness factor for the spoke-type PMSM," *IEEE Trans. Appl. Supercond.*, vol. 28, no. 3, pp. 1–5, Apr. 2018.

[16] S. Cho, H. Ahn, H. C. Liu, H.-S. Hong, J. Lee, and S.-C. Go, "Analysis of inductance according to the applied current in spoke-type PMSM and suggestion of driving mode," *IEEE Trans. Magn.*, vol. 53, no. 6, pp. 1–4, Jun. 2017.

[17] S. G. Lee, J. Bae, M. Kim, and W.-H. Kim, "Study on the improvement of the correction coefficient considering the 3-D effect of spoke-type permanent-magnet synchronous motor," *IEEE Trans. Magn.*, vol. 56, no. 3, pp. 1–5, Mar. 2020.

[18] M. Fontana and N. Bianchi, "Design and analysis of normal saliency IPM spoke motor," *IEEE Trans. Ind. Appl.*, vol. 56, no. 4, pp. 3625–3635, Jul./Aug. 2020.

[19] K.-Y. Yoon and K.-Y. Hwang, "Optimal design of spoke-type IPM motor allowing irreversible demagnetization to minimize PM weight," *IEEE Access*, vol. 9, pp. 65721–65729, 2021.

[20] Y. Xiao, Z. Q. Zhu, G. W. Jewell, J. Chen, D. Wu, and L. Gong, "A novel spoke-type asymmetric rotor interior permanent magnet machine," *IEEE Trans. Ind. Appl.*, vol. 57, no. 5, pp. 4840–4851, Sep. 2021.

[21] S. G. Lee, J. Bae, and W.-H. Kim, "Design process of spoke-type permanent magnet synchronous motor considering magnetization performance," *IEEE Trans. Appl. Supercond.*, vol. 30, no. 4, pp. 1–6, Jun. 2020.

[22] D. Konwar, P. Basumatary, U. Lee, and Y. S. Yoon, "P-doped SnFe nanocubes decorated with PdFe alloy nanoparticles for ethanol fuel cells," *J. Mater. Chem. A*, vol. 9, no. 17, pp. 10685–10694, 2021.

[23] M. Y. Kim, D. W. Chun, R. Hasan, S.-I. Kim, J.-H. Lim, S.-M. Choi, H.-S. Kim, and K. H. Lee, "Control of Cu-doping behavior in *n*-type $Cu_{0.01}Bi_{1.99}Te_{2.7}Se_{0.3}$ polycrystalline bulk via fabrication technique change," *J. Mater. Res. Technol.*, vol. 9, no. 17, pp. 765–771, Sep. 2021.

[24] S. Hong and H. Yoo, "Robust molybdenum diselenide ambipolar transistors with fluoropolymer interfacial layer and their application to complementary inverter circuits," *J. Alloys Compounds*, vol. 868, Jul. 2021, Art. no. 159212.

[25] S. Kim, H. Yoo, and S. Hong, "Lopsided-gating leads to multi-state and photo-switching behaviors with enhanced photodetections," *IEEE Sensors J.*, vol. 21, no. 20, pp. 22638–22644, Oct. 2021.

[26] S. Kahourzade, W. L. Soong, and P. Lillington, "Single-phase loading behavior of the isolated 3ph spoke interior permanent-magnet generator," *IEEE Trans. Ind. Appl.*, vol. 53, no. 3, pp. 1860–1869, May 2017.

[27] P. Eklund, J. Sjolund, M. Berg, M. Leijon, and S. Eriksson, "Experimental evaluation of a rare earth-free permanent magnet generator," *IEEE Trans. Energy Convers.*, vol. 36, no. 1, pp. 3–10, Mar. 2021.

[28] K. Li, S. Modaresahmadi, W. B. Williams, J. D. Wright, D. Som, and J. Z. Bird, "Designing and experimentally testing a magnetic gearbox for a wind turbine demonstrator," *IEEE Trans. Ind. Appl.*, vol. 55, no. 4, pp. 3522–3533, Jul. 2019.

[29] Y. Gao, R. Qu, D. Li, J. Li, and G. Zhou, "Design of a dual-stator LTS Vernier machine for direct-drive wind power generation," *IEEE Trans. Appl. Supercond.*, vol. 26, no. 4, pp. 1–5, Jun. 2016.

[30] S. J. Galioto, P. B. Reddy, A. M. El-Refaie, and J. P. Alexander, "Effect of magnet types on performance of high-speed spoke interior-permanent-magnet machines designed for traction applications," *IEEE Trans. Ind. Appl.*, vol. 51, no. 3, pp. 2148–2160, May 2015.

[31] K.-S. Lee, S.-H. Lee, J.-H. Park, J.-Y. Choi, and K.-H. Sim, "Design and experimental analysis of a 3 kW single-phase linear permanent magnet generator for stirling engines," *IEEE Trans. Magn.*, vol. 54, no. 11, pp. 1–5, Nov. 2018.

[32] Y. He, W. Zhao, H. Tang, and J. Ji, "Auxiliary teeth design to reduce short-circuit current in permanent magnet generators," *CES Trans. Electr. Mach. Syst.*, vol. 4, no. 3, pp. 198–205, Sep. 2020.

[33] D. Zhu, R. Wang, C. Liu, and J. Duan, "Synchronization of chaotic-oscillation permanent magnet synchronous generators networks via adaptive impulsive control," *IEEE Trans. Circuits Syst. II, Exp. Briefs*, vol. 67, no. 10, pp. 2194–2198, Oct. 2020.

[34] (Accessed: May 8, 2021). *Hitachi Metal, Ferrite Magnet Demagnetization Curve*. [Online]. Available: https://www.automate.org/userAssets/a3/a3Uploads/pdf/Hitachi-Magnet-Handbook.pdf

[35] D.-K. Woo and B. H. Jeong, "Irreversible demagnetization of permanent magnet in a surface-mounted permanent magnet motor with overhang structure," *IEEE Trans. Magn.*, vol. 52, no. 4, pp. 1–6, Apr. 2016.

[36] Y. Kong, M. Lin, M. Yin, and L. Hao, "Rotor structure on reducing demagnetization of magnet and torque ripple in a PMa-synRM with ferrite permanent magnet," *IEEE Trans. Magn.*, vol. 54, no. 11, Nov. 2018, Art. no. 8108705.

[37] M. Z. Islam, A. Arafat, S. S. R. Bonthu, and S. Choi, "Design of a robust five-phase ferrite-assisted synchronous reluctance motor with low demagnetization and mechanical deformation," *IEEE Trans. Energy Convers.*, vol. 34, no. 2, pp. 722–730, Jun. 2019.

DONG-HO KIM (Student Member, IEEE) received the B.S. and M.S. degrees in energy IT from Gachon University, Seongnam, South Korea, in 2017 and 2020, respectively. He is currently pursuing the Ph.D. degree with the Department of Electric Engineering, Hanyang University, Seoul, South Korea. His research interests include design and analysis of motors and generators. Applications are vehicles, home appliances, and industrial electrical machinery.

KWANG SOO KIM (Member, IEEE) received the B.S., M.S., and Ph.D. degrees in electrical engineering from Hanyang University, Seoul, South Korea, in 2005, 2007, and 2011, respectively. From 2011 to 2017, he was a Research Staff Member with the Samsung Advanced Institute of Technology, Suwon, South Korea. Since 2018, he has been an Assistant Professor with the Smart Mobility Engineering Department, Halla University, Wonju, South Korea. His research interests include design and analysis of motors and generators. Applications are vehicles, home appliances, and industrial electrical machinery.

JU LEE (Senior Member, IEEE) received the M.S. degree from Hanyang University, Seoul, South Korea, in 1988, and the Ph.D. degree in electrical engineering from Kyusyu University, Japan, in 1997. In 1997, he joined Hanyang University, where he is currently a Professor with the Department of Electrical and Bio-Engineering. His main research interests include electric machinery and its drives, electro-magnetic field analysis, transportation systems, such as hybrid electric vehicles and railway propulsion systems. He is a member of the IEEE Industry Applications Society, the Magnetics Society, and the Power Electronics Society.

IN-JUN YANG (Student Member, IEEE) received the B.S. and M.S. degrees in energy IT from Gachon University, Seoul, South Korea, in 2018 and 2020, respectively. He is currently pursuing the Ph.D. degree with the Department of Electric Engineering, Hanyang University, Seoul. His research interests include design and analysis of motors and generators. Applications are vehicles, home appliances, and industrial electrical machinery.

WON-HO KIM (Member, IEEE) received the B.S., M.S., and Ph.D. degrees in electrical engineering from Hanyang University, Seoul, South Korea, in 2005, 2007, and 2011, respectively.

From 2011 to 2017, he was a Research Staff Member with the Samsung Advanced Institute of Technology, Yongin, South Korea. Since 2017, he has been an Assistant Professor with the Electrical Engineering Department, Gachon University, Seongnam, South Korea. His research interests include design and analysis of motors and generators. Applications are vehicles, home appliances, and industrial electrical machinery.

• • •